



**Universiteit
Leiden**
The Netherlands

DNL104, a centrally penetrant RIPK1 inhibitor, inhibits RIP1 kinase phosphorylation in a randomized phase I ascending dose study in healthy volunteers

Grievink, H.W.; Heuberger, J.A.A.C.; Huang, F.; Chaudhary, R.; Birkhoff, W.A.J.; Tonn, G.R.; ... ; Groeneveld, G.J.

Citation

Grievink, H. W., Heuberger, J. A. A. C., Huang, F., Chaudhary, R., Birkhoff, W. A. J., Tonn, G. R., ... Groeneveld, G. J. (2020). DNL104, a centrally penetrant RIPK1 inhibitor, inhibits RIP1 kinase phosphorylation in a randomized phase I ascending dose study in healthy volunteers. *Clinical Pharmacology & Therapeutics*, 107(2), 406-414. doi:10.1002/cpt.1615




Version: Publisher's Version

License: [Creative Commons CC BY 4.0 license](https://creativecommons.org/licenses/by/4.0/)

Downloaded from: <https://hdl.handle.net/1887/3278292>

Note: To cite this publication please use the final published version (if applicable).

DNL104, a Centrally Penetrant RIPK1 Inhibitor, Inhibits RIP1 Kinase Phosphorylation in a Randomized Phase I Ascending Dose Study in Healthy Volunteers

Hendrika W. Grievink^{1,†} , Jules A.A.C. Heuberger^{1,†} , Fen Huang², Rinkal Chaudhary², Willem A.J. Birkhoff¹ , George R. Tonn², Sofia Mosesova², Rebecca Erickson², Matthijs Moerland¹, Patrick C.G. Haddick², Kimberly Scarce-Levie², Carole Ho² and Geert Jan Groeneveld^{1,*}

Receptor-interacting serine/threonine-protein kinase 1 (RIPK1) regulates inflammation, cytokine release, and necroptotic cell death and is implicated in pathogenic cellular pathways in amyotrophic lateral sclerosis (ALS), Alzheimer's disease (AD), and multiple sclerosis. Inhibition of RIPK1 activity protects against inflammation and cell death in multiple animal models. DNL104 is a selective, brain-penetrant inhibitor of RIPK1 phosphorylation in clinical development for AD and ALS. DNL104 was tested in 68 healthy volunteers to investigate safety and tolerability, pharmacokinetic profile in plasma and cerebrospinal fluid, and pharmacodynamic effects of RIPK1 inhibition in peripheral blood mononuclear cells in a first-in-human, placebo-controlled, double-blind, randomized single-ascending dose (SAD) and multiple-ascending dose (MAD) study. DNL104 was well-tolerated in the SAD group and during the dosing period of the MAD group. However, postdose liver toxicity in 37.5% of subjects was observed in the MAD, and assessed to be drug related. We demonstrate that DNL104 leads to RIP1 kinase inhibition, and this is not associated with central nervous system (CNS) toxicities, supporting future development of CNS penetrant RIPK1 inhibitors.

Study Highlights

WHAT IS THE CURRENT KNOWLEDGE ON THE TOPIC?

✓ Inhibition of receptor-interacting serine/threonine-protein kinase 1 (RIPK1) phosphorylation shows protection against pathology and inflammation *in vitro* and in animal studies induced by diverse challenges, including in central nervous system (CNS) disease (Alzheimer's disease and amyotrophic lateral sclerosis) animal models.

WHAT QUESTION DID THIS STUDY ADDRESS?

✓ The safety, tolerability, pharmacokinetic and pharmacodynamic effects of CNS-penetrant RIP1 kinase inhibitor DNL104 were tested in randomized placebo controlled single-ascending dose and multiple-ascending dose (MAD) trials.

WHAT DOES THIS STUDY ADD TO OUR KNOWLEDGE?

✓ The results show that DNL104 inhibits RIPK1 phosphorylation in healthy human volunteers without CNS safety effects, but there are some concerns about liver toxicity in the MAD study, where 37.5% of the subjects (six subjects) developed elevated liver function tests that were drug-related, of which 50% (three subjects) were classified as drug-induced liver injury.

HOW MIGHT THIS CHANGE CLINICAL PHARMACOLOGY OR TRANSLATIONAL SCIENCE?

✓ CNS-penetrant inhibition of RIPK1 phosphorylation is a promising way of preventing brain inflammation and necroptosis *in vivo*.

Receptor-interacting serine/threonine-protein kinase 1 (RIPK1) is an intracellular protein involved in the regulation of inflammation and cell death. RIPK1 is activated in response to several inflammatory stimuli, notably tumor necrosis factor alpha (TNF- α)

signaling through the TNF receptor 1. When activated, RIPK1 becomes phosphorylated and physically interacts with a complex of proteins, including RIPK3 and mixed lineage kinase domain-like pseudokinase. The resulting complex triggers multiple

¹Centre for Human Drug Research, Leiden, The Netherlands; ²Denali Therapeutics, South San Francisco, California, USA. *Correspondence: Geert Jan Groeneveld (GGroeneveld@chdr.nl)

[†]These authors contributed equally to this work.

Received December 20, 2018; accepted June 6, 2019. doi:10.1002/cpt.1615

cellular responses, including cytokine release, microglial activation, and necroptosis, a regulated form of cell death.^{1,2} RIPK1's early role in this signaling cascade has led to the hypothesis that inhibition of RIPK1 signaling could be beneficial in diseases that are characterized by excess cell death and inflammation. Indeed, inhibition of RIPK1 activity has been shown to protect against necroptotic cell death *in vitro* across a range of cell death models.^{3–8} In animal models of diseases ranging from ulcerative colitis to multiple sclerosis, inhibition of this pathway protects against pathology and cell death.^{4,8–15} These nonclinical findings, coupled with observations of increased RIPK1 activity in human diseases, including amyotrophic lateral sclerosis, Alzheimer's disease, and multiple sclerosis, suggest that inhibition of RIPK1 could be beneficial in many different chronic diseases.^{8,12,16,17} RIPK1 inhibitors are currently being evaluated as therapies for systemic inflammatory diseases, including inflammatory bowel disease and psoriasis,¹⁸ but there is no evidence that the inhibitors previously studied in humans penetrate into the central nervous system (CNS). To evaluate the potential of RIPK1 inhibition as a therapeutic for chronic neurodegenerative diseases, it is necessary to investigate the pharmacokinetics (PKs), pharmacodynamics (PDs), and safety profile of a molecule that is able to enter the CNS at effective concentrations.

DNL104 is a selective CNS penetrable inhibitor of RIPK1 activity developed by Denali Therapeutics (South San Francisco, CA) as a potential treatment of neurodegenerative disease. Preclinically, DNL104 inhibition of RIPK1 signaling was demonstrated by its ability to block downstream effects of acute TNF- α stimulation in rodents, including increased RIPK1 phosphorylation, cytokine release, and hypothermia. In human peripheral blood mononuclear cells (PBMCs) stimulated by TNF- α *ex vivo*, DNL104 blocked the resulting phosphorylation of RIPK1 at serine 166 in a concentration-dependent manner.

This paper reports the outcome of the phase I study of DNL104, assessing the tolerability, safety, and PK and PD profiles in healthy volunteers in a single-ascending dose (SAD) study as well as a multiple-ascending dose (MAD) study. Although postdose alterations in liver function tests assessed to be unrelated to RIPK1 target inhibition were observed that precluded the further development of DNL104, concentrations expected to fully inhibit the kinase in the CNS were achieved in the absence of any reported CNS-associated toxicities. These data support the continued development of this class of inhibitors for neurodegenerative disease.

RESULTS

Demographics

Demographics and baseline characteristics were comparable among the active and placebo treatment groups with the exception of an age imbalance in the MAD study (placebo-treated subjects averaged about 10 years younger than those treated with DNL104). The median age of subjects receiving single doses was 31.5 years (range: 18–63 years), and most were men (92%) and white (77%). The median age of the subjects receiving multiple doses was 30 years (range: 20–48 years). All of these subjects were men, and the majority was white (80%). The demographics per treatment group are summarized in **Table 1**.

Table 1 Age, race, and sex of included subjects in the SAD and MAD studies

	SAD placebo	SAD 5 mg	SAD 15 mg	SAD 50 mg	SAD 100 mg (+75 mg fed)	SAD 150 mg	SAD 225 mg	MAD placebo	MAD 50 mg	MAD 100 mg
N	12	6	6	6	6	6	6	4	8	8
Age (median, Q1, Q3)	27 (23, 50.75)	39 (20.5, 59.25)	32 (24.75, 44.5)	30 (21.75, 57.75)	47.5 (24, 51)	41.5 (21.5, 58.75)	30.5 (25.75, 42.75)	24 (20.50, 26.75)	30 (27.5, 35.5)	30.5 (21.75, 43.75)
Race (% white)	75	100	83.3	66.6	83.3	66.6	66.6	100	75	75
Sex (% male)	100	83.3	100	83.3	83.3	83.3	100	100	100	100

MAD, multiple-ascending dose; SAD, single-ascending dose.

Table 2 Geometric mean, geometric %CV (arithmetic mean \pm SD) DNL104 plasma pharmacokinetic parameters following a single dose to healthy subjects

Dose (mg)	5	15	50	75	100	150	225
Feeding status	Fasted	Fasted	Fasted	Fed	Fasted	Fasted	Fasted
N	6	6	6	6	6	6	6
C_{max} (nmol/L)	61.4, 18.8% (62.4 \pm 13.2)	169, 53.1% (186 \pm 79.8)	395, 86.4% (474 \pm 250)	542, 49.9% (594 \pm 277)	1,530, 56.6% (1,730 \pm 1,000)	1,990, 36.1% (2,090 \pm 714)	3,630, 34.5% (3,810 \pm 1,300)
T_{max}^a (hour)	1.29 (0.517–2.00) (1.27 \pm 0.513)	1.50 (1.00–2.00) (1.5 \pm 0.447)	2.00 (1.50–4.00) (2.25 \pm 0.880)	4.00 (2.00–4.00) (3.67 \pm 0.816)	1.50 (1.00–4.00) (1.83 \pm 1.13)	1.75 (1.00–2.00) (1.58 \pm 0.492)	1.50 (1.00–4.00) (1.83 \pm 1.13)
Half-life (hour)	2.60, 22.1% (2.66 \pm 0.632)	2.29, 40.5% (2.46 \pm 1.22)	2.26, 42.5% (2.46 \pm 1.31)	3.49, 27.3% (3.60 \pm 0.973)	3.07, 38.5% (3.23 \pm 0.980)	2.93, 33.0% (3.04 \pm 0.808)	4.13, 15.6% (4.17 \pm 0.644)
AUC _{0–inf} (nmol hour/L)	225, 27.1% (231 \pm 54.1)	641, 63.3% (740 \pm 465)	1,830, 23.7% (1,880 \pm 444)	4,200, 67.8% (4,870 \pm 2,910)	5,710, 64.1% (6,710 \pm 4,710)	7,080, 35.7% (7,460 \pm 2,740)	20,300, 23.3% (20,700 \pm 4,470)
CL/F (L/hour)	75.2, 27.1% (77.6 \pm 23.2)	79.2, 63.3% (90.4 \pm 50.2)	92.2, 23.7% (94.3 \pm 21.4)	60.4, 67.8% (69.8 \pm 40.1)	59.2, 64.1% (66.8 \pm 31.0)	71.7, 35.7% (75.1 \pm 23.4)	37.5, 23.3% (38.4 \pm 9.34)
Vz/F (L)	282, 19.1% (287 \pm 53.5)	261, 38.8% (278 \pm 115)	301, 61.0% (351 \pm 248)	304, 51.8% (334 \pm 157)	263, 48.7% (285 \pm 116)	303, 26.0% (311 \pm 78.3)	223, 15.2% (226 \pm 35.4)
CSF to plasma ratio	NA	NA	NA	NA	NA	0.197, 8.14% (0.197 \pm 0.0157)	0.154, 17.5% (0.156 \pm 0.0254)

%CV, percentage of coefficient of variation; AUC_{0–inf}, area under the urinary excretion rate curve from 0 hour to infinity; CL/F, apparent clearance (clearance, CL, divided by bioavailability, F); C_{max} , peak plasma concentration; CSF, cerebrospinal fluid; NA, not applicable; T_{max} , time of maximum plasma concentration; Vz/F, apparent volume of distribution (volume of distribution based on the terminal phase, Vz, divided by bioavailability, F).

^a T_{max} reported as median (minimum to maximum) (arithmetic mean \pm SD).

Safety

Single doses of DNL104 were well-tolerated and no significant drug-related safety concerns were observed up to the highest dose of 225 mg. In total, 42 treatment-emergent adverse events (TEAEs) were reported for 25 subjects (52.1% of total), of which 50% were considered possibly treatment-related. Most TEAEs were mild. Two moderately intense TEAEs were reported (one case of myalgia and one of postlumbar puncture headache, both considered nondrug related) and no severe TEAEs were reported. No dose-related pattern of adverse events (AEs) was noted. No serious adverse events or discontinuations due to TEAEs occurred in the SAD study. No significant laboratory abnormalities were observed. TEAEs that were observed in at least two subjects are summarized in **Table 2**.

In the MAD study, 51 TEAEs in total were reported during the study period. At least one TEAE was reported by all 4 of the subjects in the placebo group and 12 (75%) subjects in the DNL104-treated groups. The most frequently reported events in combined active and placebo subjects were headache (eight subjects), dizziness and somnolence (three subjects each), and nausea, application site irritation, back pain, paresthesia, and feeling hot (two subjects each). There was no pattern of incidence of these events seen across the treatment groups. One of the TEAEs was of moderate intensity (abnormal liver function test that emerged after the end of dosing and lasted 35 days in one subject treated with 50 mg DNL104); the others were classified as mild. However, elevations in liver function tests were subsequently found for five additional subjects receiving DNL104 in the MAD study (**Figure 1**). Three of the six subjects had mild AST and ALT increases, of which one occurred during the dosing period ($1.5 \times$ upper limit of normal (ULN) for ALT). These parameters returned to normal by day 50

(at the latest) after the first dosing day. However, three subjects had substantial increases in ALT (15-fold, 2.7-fold, and 3.2-fold ULN, respectively) and AST (6-fold, 1.1-fold, and 2-fold ULN, respectively), all occurring after the last dose had been administered. One of these subjects had an increased lactate dehydrogenase (1.2-fold ULN) with a gamma GT that was within normal limits, but which had increased threefold from the baseline measurement. Alkaline phosphatase did increase in two of three subjects, but stayed within normal limits, with peak levels of 115 U/L, 82 U/L, and 111 U/L, respectively. The R-ratio (the ratio between ALT and alkaline phosphatase) was > 5 for 1 subject and > 2 for the other 2 subjects. An R-ratio of > 5 indicates hepatocellular drug-induced liver injury (DILI), whereas an R-ratio > 2 indicates a mix of cholestatic and hepatocellular injury. One subject experienced nausea and malaise. All three subjects also had elevated eosinophil counts (1.9-fold, 2-fold, and 2-fold of ULN, or 23.5%, 26.8%, and 11.1% of total leukocytes, respectively) and IgE levels (1.8-fold, 2.2-fold, and 4.9-fold of ULN, respectively). All values returned to normal within 60 days after the first dose. Bilirubin, coagulation markers, IgG levels, and virology (hepatitis, Epstein Barr virus, and cytomegalovirus), as well as drug toxicity screenings remained normal for all subjects, and no rash, fever, or facial edema was observed. Although all subjects recovered without sequelae, a third planned cohort at a higher dose was canceled due to these observed AEs.

PK data

In the SAD study, the median time of maximum plasma concentration (T_{max}) values in fasted subjects varied from 1.29 to 2 hours for the different doses (see **Table 2**). Following peak plasma concentration (C_{max}), DNL104 plasma concentrations declined in a monophasic or biphasic manner with a terminal life that ranged

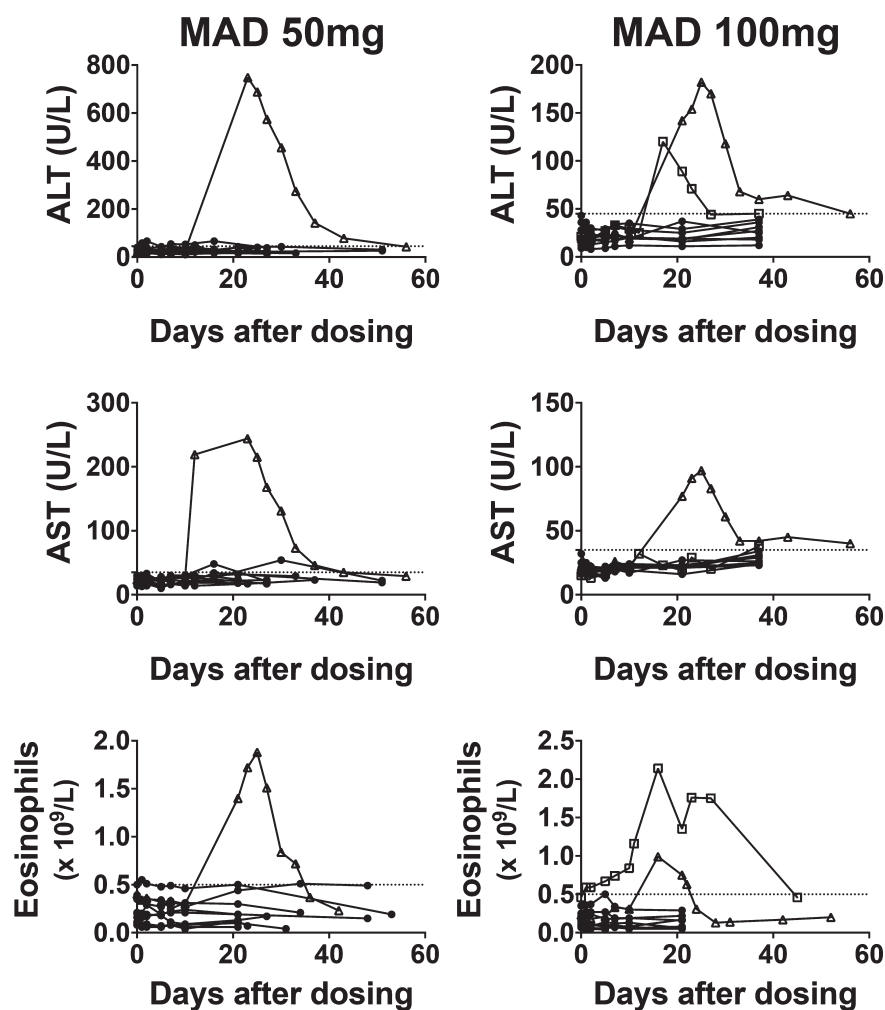


Figure 1 Laboratory abnormalities in the multiple-ascending dose (MAD) cohorts. ALT, AST and eosinophils counts results are shown for the MAD cohorts receiving 50 mg and 100 mg doses, respectively. The x-axis depicts the days after first dose. The subjects showing abnormalities were followed until the results were back to normal. The upper limit of the reference range is shown as a dashed line on the y-axis. Note that the range of the y-axis is not the same for each pair of graphs.

between 1.53 and 5.12 hours. Half-life seemed to be independent of dose. Over the dose range in the study, the C_{max} of DNL104 increased in a dose proportional manner, whereas area under the concentration-time curve from zero to infinity ($AUC_{0-\infty}$) increased in a slight but statistically greater than dose proportional manner (i.e., based on regression analysis $AUC_{0-\infty}$ increases 2.19-fold for a 2-fold increase in dose). Administration of DNL104 with food (i.e., high-fat breakfast) did not affect the half-life or the dose normalized area under the concentration-time curve from time of administration up to the time of the last quantifiable concentration (AUC_{0-last}) and $AUC_{0-\infty}$; however, T_{max} seemed delayed, and the dose normalized C_{max} was reduced. This data suggests that coadministration of DNL104 with food delayed the absorption rate but not the extent of absorption. PK profiles of the different doses and food cohort can be seen in Figure 2.

The renal elimination of DNL104 is a minor route of clearance with the maximum percentage of the dose excreted unchanged in the urine being 0.143%. The renal clearance was also small with a maximum value of 0.0663 L/hour.

Cerebrospinal fluid (CSF) concentrations at 6 hours postdose were lower than the corresponding plasma concentrations and ranged from 35.3–137 nmol/L following a 150 mg dose and

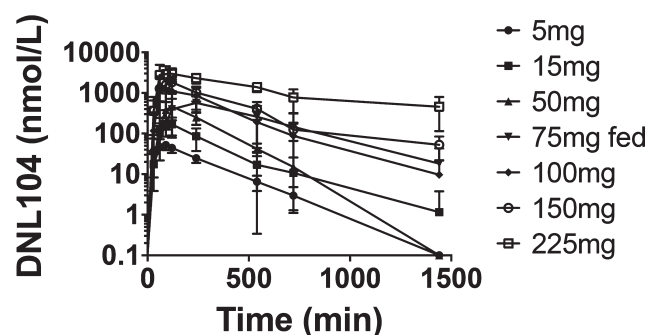


Figure 2 Pharmacokinetics of DNL104. DNL104 concentration was measured in plasma collected at multiple times after DNL104 administration to create a pharmacokinetic profile of DNL104 in the single-ascending dose cohort, including a group administered 75 mg of DNL104 with food.

Table 3 Geometric mean, geometric %CV (arithmetic mean \pm SD) DNL104 plasma pharmacokinetic parameters following a single dose to healthy subjects

Dose (mg)	5	15	50	75 ^a	100 ^a	150	225
Feeding status	Fasted	Fasted	Fasted	Fed	Fasted	Fasted	Fasted
N	6	6	6	6	6	6	6
C _{max} (nmol/L)	61.4, 18.8% (62.4 \pm 13.2)	169, 53.1% (186 \pm 79.8)	395, 86.4% (474 \pm 250)	542, 49.9% (594 \pm 277)	1,530, 56.6% (1,730 \pm 1,000)	1,990, 36.1% (2,090 \pm 714)	3,630, 34.5% (3,810 \pm 1,300)
T _{max} ^b (hour)	1.29 (0.517–2.00) (1.27 \pm 0.513)	1.50 (1.00–2.00) (1.5 \pm 0.447)	2.00 (1.50–4.00) (2.25 \pm 0.880)	4.00 (2.00–4.00) (3.67 \pm 0.816)	1.50 (1.00–4.00) (1.83 \pm 1.13)	1.75 (1.00–2.00) (1.58 \pm 0.492)	1.50 (1.00–4.00) (1.83 \pm 1.13)
Half-life (hour)	2.60, 22.1% (2.66 \pm 0.632)	2.29, 40.5% (2.46 \pm 1.22)	2.26, 42.5% (2.46 \pm 1.31)	3.49, 27.3% (3.60 \pm 0.973)	3.07, 38.5% (3.23 \pm 0.980)	2.93, 33.0% (3.04 \pm 0.808)	4.13, 15.6% (4.17 \pm 0.644)
AUC _{0–inf} (nmol hour/L)	225, 27.1% (231 \pm 54.1)	641, 63.3% (740 \pm 465)	1,830, 23.7% (1,880 \pm 444)	4,200, 67.8% (4,870 \pm 2,910)	5,710, 64.1% (6,710 \pm 4,710)	7,080, 35.7% (7,460 \pm 2,740)	20,300, 23.3% (20,700 \pm 4,470)
CL/F (L/hour)	75.2, 27.1% (77.6 \pm 23.2)	79.2, 63.3% (90.4 \pm 50.2)	92.2, 23.7% (94.3 \pm 21.4)	60.4, 67.8% (69.8 \pm 40.1)	59.2, 64.1% (66.8 \pm 31.0)	71.7, 35.7% (75.1 \pm 23.4)	37.5, 23.3% (38.4 \pm 9.34)
Vz/F (L)	282, 19.1% (287 \pm 53.5)	261, 38.8% (278 \pm 115)	301, 61.0% (351 \pm 248)	304, 51.8% (334 \pm 157)	263, 48.7% (285 \pm 116)	303, 26.0% (311 \pm 78.3)	223, 15.2% (226 \pm 35.4)
CSF to plasma ratio	NA	NA	NA	NA	NA	0.197, 8.14% (0.197 \pm 0.0157)	0.154, 17.5% (0.156 \pm 0.0254)

%CV, percentage of coefficient of variation; AUC_{0–inf}, area under the urinary excretion rate curve from 0 hour to infinity; CL/F, apparent clearance (clearance, CL, divided by bioavailability, F); C_{max}, peak plasma concentration; CSF, cerebrospinal fluid; NA, not applicable; T_{max}, time of maximum plasma concentration; Vz/F, apparent volume of distribution (volume of distribution based on the terminal phase, Vz, divided by bioavailability, F).

^a The food effect cohort was performed in a crossover design, and the same subjects were dosed with 100 mg DNL104 in the fasted state and 75 mg DNL104 in the fed state.

^b T_{max} reported as median (minimum to maximum; arithmetic mean \pm SD).

136–282 nmol/L following a 225 mg dose. The corresponding CSF:plasma concentration ratios ranged from 0.173–0.215 and 0.116–0.183 following the 150 and 225 mg doses, respectively. The CSF to plasma ratios were similar to the unbound fraction of DNL104 in human plasma (0.117 \pm 0.011 determined at concentrations between 0.2 and 65 μ g/mL; data on file). All PK results of the SAD are summarized in **Table 3**.

In the MAD study, T_{max} ranged to a similar extent, from 1–3.13 hours. Due to the short dosing interval in the MAD study (6 hours between the morning and afternoon dose), the half-life and derived parameters, such as AUC_{0–inf}, total apparent clearance, and accumulation index could not be accurately estimated. The time taken to reach PK steady-state assessed using the trough plasma concentrations (C_{trough}) suggest that it was achieved by the

end of the first day. C_{max}, last measurable concentration (C_{last}), and AUC_{0–last} of DNL104 following the first doses on both day 1 and day 10 increased in a dose proportional manner from 50 to 100 mg. The CSF concentration data for DNL104 at ~ 6 hours following the first oral dose of 100 mg on day 10 were lower than the corresponding plasma concentrations and ranged from 30.1–156 nmol/L. The corresponding CSF:plasma concentration ratios range from 0.129–0.235, similar to the unbound fraction of DNL104 in human plasma. All PK results of the MAD study are summarized in **Table 4**.

PD data

Reduction of pS166 RIPK1 levels in PBMCs was used to measure reduction in RIPK1 activity. To establish the measurement of RIPK1 pS166 as a PD assay *in vitro*, a concentration range of

Table 4 Geometric mean, geometric %CV (arithmetic mean \pm SD) DNL104 plasma pharmacokinetic parameters following the first oral dose on days 1 and 10 (doses 1 and 28) following dosing 3 times a day for 10 days to healthy subjects

Dose (mg)	50	100	50	100
Dose number	1	1	28	28
C _{max} (nmol/L)	N = 8 550, 50.1% (606 \pm 285)	N = 8 1,220, 58.5% (1,380 \pm 741)	N = 8 547, 40.6% (585 \pm 233)	N = 8 1,360, 57.9% (1,540 \pm 777)
T _{max} ^a (hour)	N = 8 3.00 (1.00–3.13) (2.33 \pm 0.976)	N = 8 3.00 (1.00–3.07) (2.57 \pm 0.826)	N = 8 1.54 (1.50–3.00) (2.07 \pm 0.768)	N = 8 3.00 (1.02–3.03) (2.57 \pm 0.819)
CSF to plasma ratio	NA	NA	NA	0.173, 21.4% (0.177 \pm 0.0375)

%CV, percentage of coefficient of variation; C_{max}, peak plasma concentration; NA, not applicable; T_{max}, time of maximum plasma concentration.

^a T_{max} reported as median (minimum to maximum) (arithmetic mean \pm SD).

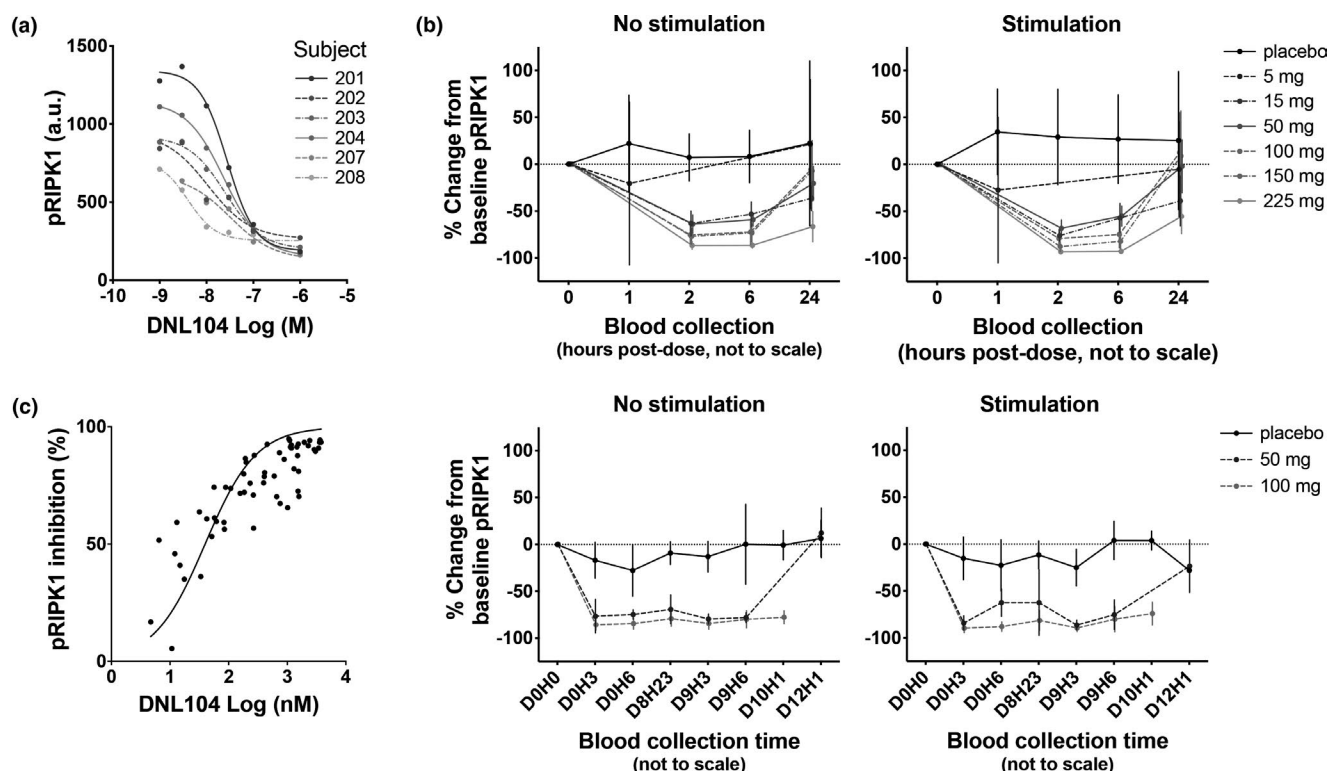


Figure 3 Pharmacodynamics of DNL104. Peripheral blood mononuclear cells are incubated with a dose range of DNL104 ($n = 6$) to determine the half-maximal inhibitory concentration (IC_{50}) of DNL104 *ex vivo* (a). Receptor-interacting serine/threonine-protein kinase 1 (RIPK1) phosphorylation is measured by Meso Scale Discovery (arbitrary units) in the single-ascending dose (SAD) and multiple-ascending dose (MAD) cohorts (b). The change from baseline RIPK1 phosphorylation without (left) or with (right) pan-caspase inhibitor zVAD-FMK stimulation is shown for the different doses in the SAD cohort (upper panels) and MAD cohort (lower panels). Total DNL104 plasma concentrations from the SAD cohort are plotted on the x-axis with relative pRIPK1 inhibition at the same time points on the y-axis to determine the IC_{50} *in vivo* (c).

DNL104 was spiked into PBMCs taken from healthy donors. A cocktail of TNF- α , the second mitochondria-derived activator of caspase mimetic SM-164, and the pan-caspase inhibitor zVAD-FMK (TSZ) was used to stimulate the cells to increase pRIPK1. The geometric mean half-maximal inhibitory concentration (IC_{50}) calculated from three biological replicates is 3.2 nM (data not shown, value not adjusted for fetal bovine serum binding). The potency of DNL104 was further validated by spiking DNL104 into PBMCs obtained before dosing from SAD cohort two subjects in the DNL104 clinical study. As shown in **Figure 3a**, the geometric mean IC_{50} calculated from 6 donors was 16.8 nM. After correcting for the 88% plasma binding of DNL104, the mean unbound IC_{50} is 1.97 nM, which is in good accordance with the previously calculated unbound *in vitro* PBMC IC_{50} (2.4 nM, adjusted for fetal bovine serum binding 24%).

To measure PD response in the clinic, the same pS166 RIPK1 assay was used to measure the levels of RIPK1 activity at specific postdose time points in PBMCs isolated from volunteers in both the SAD and MAD studies. An aliquot of PBMCs was stimulated with TSZ to increase pRIPK1 levels, but pRIPK1 was also measured in unstimulated PBMCs in order to better reflect the *in vivo* physiology. In the absence of DNL104, absolute RIPK1 phosphorylation varied both between individuals and within individuals over time. To assess the effects of inhibition, the levels of RIPK1 phosphorylation at each time point were

normalized to each individual's predose pRIPK1 level. In the SAD study, a single dose of DNL104 dose-dependently inhibited RIPK1 phosphorylation in both nonstimulated and TSZ-stimulated PBMCs (**Figure 3b**). At the highest dose (225 mg), an inhibition of up to 80% was observed at 2–6 hours after dosing, whereas after 24 hours an inhibition of 50% was observed. In the MAD study, thrice daily DNL104 doses of 50 mg or 100 mg resulted in 50% to > 90% inhibition and 70% to > 90%, respectively, at steady-state (**Figure 3b**).

The inhibition of RIPK1 phosphorylation in PBMCs is strongly related to DNL104 plasma concentration (**Figure 3c**, based on stimulated/unstimulated pRIPK1 levels). The calculated IC_{50} was 39.71 ± 1.15 nM SE without correction for plasma binding, which is in good accordance with the *in vitro* PBMC IC_{50} value.

DISCUSSION

The main goal of the first-in-human study of DNL104 was to assess safety and tolerability. Although DNL104 was well tolerated in the SAD part of the study and during the dosing period of the MAD study, liver toxicity was observed in six subjects treated with DNL104 (37.5%), of which three classified as DILI.¹⁹ One subject showed an increase in ALT ($1.5 \times$ ULN) during the 10-day dosing period, which returned to normal at the end of the dosing period, and five other subjects showed an increase in liver function markers only after the end of the

dosing period. Of these five subjects, three subjects (18.8% of those treated with multiple doses of DNL104) showed an increase in ALT and AST well above the normal upper limits and also had eosinophilia and elevated IgE levels, indicative of DILI. The calculated R-ratio was also > 2 for all subjects. To rule out other causes, the Roussel Uclaf Causality Assessment Method and Maria and Victorino causality assessments were performed.^{20,21} No indication of alcoholism, viral hepatitis, or autoimmunity were found. It is unlikely that the observed liver toxicity is a consequence of RIPK1 inhibition because there were no AE reports indicating liver toxicity in 60 subjects dosed with GSK2982772, a selective RIPK1 inhibitor,¹⁸ and there are no reported liver abnormalities in RIPK1 dead mice.^{22–24}

Preclinical toxicity studies of DNL104 in rats and dogs identified hepatobiliary impairment as the predominant finding. DNL104 was generally well tolerated up to doses of 100 mg/kg in rats ($C_{\max} = 47 \mu\text{M}$; 0–24-hour area under the concentration-time curve (AUC_{0-24}) = 262 μM hour) and 30 mg/kg in dogs ($C_{\max} = 35 \mu\text{M}$; $\text{AUC}_{0-24} = 62 \mu\text{M}$ hour), but at doses above this, adverse histopathological changes were noted in the liver and/or gall bladder. The histopathological changes in the liver included single cell necrosis/apoptosis, associated with inflammatory mixed cell infiltrates, hepatocellular hypertrophy, and/or increased cytoplasmic vacuolation of the bile ducts (see **Figure S1** and **Supplemental Information** for methods). At the highest doses, these findings were consistent with a mild cholestasis and included minimal-to-mild increases in ALT and total bilirubin in rats and dogs (~ 1.5 -fold to 3-fold baseline and/or control levels) and gamma glutamyltransferase in rats only (6-fold to 21-fold); however, there were no changes in eosinophil counts or total globulins (immunoglobulins were not subtyped). The most sensitive preclinical species was dog, which provided a fivefold safety margin (dog AUC_{0-24} at the no observed adverse effects level divided by human AUC_{0-24} at 100 mg t.i.d.), indicating that humans may be more sensitive to DNL104-induced hepatotoxicity. Together, these findings along with elevated levels of ALT, AST, eosinophils, IgE, and the absence of other possible explanations are consistent with this being a late-onset DILI, most likely caused by an immunoallergic reaction to DNL104 or its metabolites. Because bilirubin and coagulation markers remained normal, and the R-ratio was > 2 and in one case > 5 , the DILI observed in these three subjects can be classified as hepatocellular. Because of these AEs, it was decided to not escalate the dose any further.

Although DILI is a well-known adverse effect of drugs, such as acetaminophen,²⁵ antibiotics,²⁶ and antiretroviral agents,²⁷ DILI due to hypersensitivity is a rare event that has been described in case studies.²⁸ However, a recent publication by Jin *et al.*²⁹ describes a similar pattern in a multiple-dose study of LY3031207, a microsomal prostaglandin E synthase 1 inhibitor. A comparable elevation in liver enzymes was seen, as well as eosinophilia and increased IgE levels. In this case, a delayed onset of DILI (after multiple doses) was observed as well. In the case of LY3031207, the suggested explanation for toxicity was the formation of reactive metabolites, which were present in the plasma and urine.²⁹ Although a delayed onset of DILI has been described before, it has been indicated that RIPK1 inhibition

may protect against hepatotoxicity,^{30–32} potentially supporting an explanation for the delayed onset of DNL104-related findings in the postdosing period.

In terms of PK, DNL104 showed acceptable characteristics. The terminal half-life was between 1.53 and 5.12 hours in the SAD study, therefore, the dosing schedule for the MAD study was set at three doses per day to keep plasma levels above $\sim 250 \text{ nM}$ /L, concentrations projected to achieve 90% RIPK1 inhibition based on the PBMC IC_{50} . Minimal influence of a high-fat diet was observed. Therefore, dosing was done nonfasted, except on the 1st and 10th days of dosing to get similar PK patterns to the SAD study. Although the half-life was shorter than expected, the PK properties of DNL104 were considered acceptable for further development.

Reduction of phosphorylation of RIPK1 in PBMCs isolated from the subjects was used as a measure of target engagement. Once TNF- α binds the TNF receptor 1, the intracellular domain of TNFR1 starts the recruitment of the adaptor TNFR1-associated death domain protein TRADD, which recruits RIPK1 and two ubiquitin ligases: TRAF2 and cIAP1, which mediate ubiquitination of RIPK1 resulting in formation of stable complex I and initiating cell survival pathway, including NF- κB activation.³³ When cIAP1 and cIAP2 are depleted by the second mitochondria-derived activator of caspase mimetics (SM-164) and caspase-8 is inhibited by zVAD-FMK, autophosphorylation of RIPK1 at serine 166 increases and allows RIPK1 to form complex IIb with RIPK3 and MLKL to induce necroptosis. The modulation of RIPK1 S166 autophosphorylation is a sensitive and specific measure of RIPK1 activity in acute settings.

In both the SAD and MAD studies, at DNL104 doses exceeding 15 mg, clear RIPK1 phosphorylation inhibition was observed. When individual plasma DNL104 concentrations were compared with RIPK1 inhibition, a strong concentration–response relationship was observed, indicating that pRIPK1 levels in PBMCs are a useful measure of peripheral target engagement. After correction for plasma protein binding, the IC_{50} calculated from the measured plasma DNL104 concentrations and PBMC pRIPK1 levels (1.96 nM) agreed well with the calculated *in vitro* IC_{50} of 2.4 nM. Interestingly, similar inhibition of pRIPK1 in the PBMCs of volunteers dosed with DNL104 was observed in both the absence and presence of TSZ stimulation (**Figure 3b**).

Given that DNL104 was in development for treatment of amyotrophic lateral sclerosis and Alzheimer's disease, DNL104 was selected for its CNS penetrant properties. The concentration of DNL104 in CSF was 15% of the plasma concentrations. This is in agreement with the free fraction of DNL104 (11.7%); 88% of DNL104 is bound by plasma proteins, but CSF has much lower protein levels. Because the PBMC RIPK1 phosphorylation assay reflects the effects of unbound DNL104, the DNL104 dose resulting in maximal target inhibition in the PBMC-based assay can be expected to correspond to the CSF unbound concentrations required to modulate RIPK1 activity in the CNS.

In summary, increasing doses of DNL104 significantly inhibited RIPK1 phosphorylation and demonstrated CNS penetrant properties, thus supporting the utility of this class of therapeutics for future therapeutic application in neurodegenerative diseases

via interference in necroptotic and neuroinflammatory pathways. The compound was detected at pharmacologically active concentrations in CSF, which is key to the anticipated mechanism of action of the compound in the CNS. Aside from the liver abnormalities observed in the MAD cohort, which are assessed to be off-target, no meaningful changes were noted in hematology, serum chemistry, urinalysis test results, vital signs, or electrocardiograms (ECGs). Over the dose range studied, the PK properties of DNL104 are consistent with an orally absorbed CNS penetrant small molecule. The development of DNL104 was discontinued due to the occurrence of DILI in the MAD study. However, this study demonstrated that the concept of RIPK1 inhibition, and the methodology to monitor this activity in the clinic, holds promise for future drugs targeting the RIPK1 pathway in the CNS.

METHODS

Study designs

Two phase I studies (one SAD and one MAD) were designed and conducted in a randomized, double-blind, placebo-controlled, PK/PD-guided manner in healthy adult male and female volunteers of non-childbearing potential. Subjects were dosed orally with DNL104 or a placebo. The studies were approved by the Independent Ethics Committee of the Foundation "Evaluation of Ethics in Biomedical Research" (Stichting Beoordeling Ethiek Biomedisch Onderzoek), Assen, The Netherlands. The MAD study is registered in the Dutch Trial Registry (Nederlands Trial Register (NTR)) under study number NTR6257 (MAD) and took place between January and April 2017. The SAD study took place between September and December 2016 and is not registered. All subjects signed an informed consent form prior to any study-related activity.

In total, 48 subjects were enrolled in the SAD study, and 47 of them completed the treatment period. One subject in the 100 mg cohort who was randomized to placebo received only the first dose (after fasting) and was discontinued prior to receiving the second dose (after a high-fat meal) due to a nonsustained ventricular tachycardia that was not detected on the baseline ECG. Cohorts consisted of eight subjects each, of which six were administered 5, 15, 50, 100, 150, or 225 mg, and two subjects in each cohort receiving placebo (12 subjects total). In addition, the cohort receiving 100 mg also received a 75 mg dose after receiving a high-fat meal in a crossover design. Between each cohort there was an interim analysis before escalation of the dose. For the MAD study, 20 of the 30 planned subjects were enrolled in two cohorts and randomized 4:1 to DNL104 vs. placebo: eight receiving multiple doses of 50 mg, eight receiving multiple doses of 100 mg, and four receiving placebo (2 per cohort). The multiple doses consisted of three doses each day for 10 consecutive days, with a total of 30 doses per subject. Dose escalation between all cohorts took place following a thorough review of the safety and tolerability data for at least 24 hours post-last dose and evaluation of all available PK and PD assessments of the preceding dose group.

Bioanalytical assay

DNL104 levels were measured in K3EDTA plasma, CSF, and urine. DNL104 levels were measured using validated liquid chromatography tandem mass spectrometry methods by Aptuit (Verona, Italy). The lower limit of quantification was 1.69 nmol/L.

PD assay

One day prior to dosing, blood was collected from subjects and PBMCs were isolated using cell preparation tubes containing sodium heparin (Becton Dickinson, Franklin Lakes, NJ). After centrifugation, plasma was collected and saved prior to PBMC isolation. PBMCs were washed twice with phosphate buffered saline (PBS). The isolated PBMCs were resuspended in the autologous plasma and a dose range of DNL104 was

added and incubated for 30 minutes at 37°C 5% CO₂. Subsequently, TSZ (10 ng/mL human TNF α ; R&D Systems, Abingdon, UK, #210-TA-020), 100 nM Smac mimetic SM-164 (ApexBio, Houston, TX, #A8815), and 1 μ M Z-VAD-FMK (R&D Systems, #FMK001) stimulant was added for 2 hours. After incubation, the cultures were centrifuged and supernatant was discarded. PBMCs were lysed using 1 \times RIPA lysis and subsequently centrifuged and the supernatant was frozen at -80°C until pRIPK1 assay.

For SAD and MAD cohort blood draws for PD assays, PBMCs were isolated using cell preparation tubes containing sodium heparin (Becton Dickinson). After centrifugation, plasma was collected and saved prior to PBMC isolation. PBMCs were washed twice with PBS. The isolated PBMCs were resuspended in the autologous plasma and split into two aliquots. One aliquot was incubated for 150 minutes at 37°C CO₂ and the other aliquot had TSZ stimulant added 30 minutes into a total incubation of 150 minutes at 37°C CO₂. After incubation, the cultures were centrifuged and supernatant was discarded. PBMCs were lysed using 1 \times CST lysis buffer (Cell Signaling Technologies, Leiden, the Netherlands) and subsequently centrifuged, and the supernatant was frozen at -80°C until pRIPK1 assay.

pRIPK1 assay

Serine 166 phosphorylated RIPK1 was detected with a Meso Scale Discovery (MSD) platform-based immunoassay. A streptavidin small spot 96-well plate (MSD) was coated with 1 μ g/mL of biotinylated mouse anti-RIPK1 antibody (BD Bioscience, San Jose, CA, #610459) diluted in 1 \times PBS for 1 hour at room temperature. The plate was blocked with 150 μ L blocking buffer consisting of 25% MSD blocker A in 1 \times TRIS-buffered saline-Tween-20 for 2 hours at room temperature. The 40 μ L of PBMC cell lysate was loaded to each well and incubated for 2 hours at room temperature. The detection antibody rabbit anti-pS166 RIPK1 (Cell Signaling Technology, #65746, Leiden, the Netherlands) was diluted at 400 \times in blocking buffer. The 40 μ L of diluted detection antibody was loaded to each well and incubated for 1 hour at room temperature. The secondary antibody SULFO tagged goat anti-rabbit antibody (MSD) was diluted to 1 μ g/mL in blocking buffer and incubated for 45 minutes at room temperature. The 150 μ L of 2 \times Reading Buffer T (MSD) was added to each well, and the plate was read using a Sector S 600 plate reader (MSD). The plate was washed three times with 1 \times TRIS-buffered saline-Tween-20 in a Biotek Microplate washer after each incubation step.

Data analysis

Noncompartmental PK analysis was performed using Phoenix WinNolin 6.4 (Certara USA, Princeton, NJ). Concentrations below the assay limit of quantification were treated as 0 nmol/L prior to the first sample or as missing at all other time points. PK parameters were determined as data permitted. The terminal half-life was calculated by log-linear extrapolation points determined to be on the apparent terminal phase. The AUC_{0-last} using the linear-log trapezoidal rule, which uses linear interpolation between data points prior to the C_{max} and logarithmic interpolation between points after the C_{max}. Where the terminal phase was sufficiently well characterized, the AUC_{0-inf} was determined. Dose proportionality was assessed by taking the natural logarithm of both the dose level and the PK parameter, and performing least squares regression for the line of best fit. The relationship is considered to be linear if the 95% confidence interval of the slope, which is equal to the coefficient of the equation parameter = constant \times dose^{coefficient} on the untransformed scale, contains 1. Due to the limited nature of the CSF sampling (a single paired CSF and plasma collection), only CSF to plasma ratios were calculated and reported. Based on the urine bioanalytical data, the amount of DNL104 excreted unchanged in urine, the percent of the dose excreted, and the renal clearance were calculated. Given the explorative character of the PD analysis, no formal statistical analysis was performed. For descriptive and graphical summaries, data from placebo subjects from different cohorts were pooled into a single treatment group.

The correlation between DNL104 plasma concentration and pRIPK1 inhibition was calculated using all data from the SAD study with data above quantification limits. The data were plotted in GraphPad Prism (GraphPad Software, La Jolla, CA), transformed to logarithmic values, and a nonlinear regression fit was calculated.

Safety

All subjects underwent medical screening, including medical history, physical examination, neurological examination, vital signs measurement in supine position, 12-lead ECG, urinalysis, drug screen, and safety chemistry, coagulation, and hematology blood sampling. During study periods, safety was assessed using monitoring of AEs, vital signs, ECG, physical and neurological examination, and safety chemistry, coagulation, and hematology blood sampling.

SUPPORTING INFORMATION

Supplementary information accompanies this paper on the *Clinical Pharmacology & Therapeutics* website (www.cpt-journal.com).

Supplemental Methods.

Figure S1. Dog liver histopathology findings.

ACKNOWLEDGMENTS

We thank Aptuit (Verona) for conducting the nonclinical toxicology studies and Rossella Defazio (DVM, DECVP) for data analysis and providing histopathology images.

FUNDING

The research described in this paper was funded by Denali Therapeutics Inc.

CONFLICTS OF INTEREST

The authors declared no competing interests for this work.

AUTHOR CONTRIBUTIONS

H.W.G., P.C.G.H., J.A.A.C.H., M.M., G.J.G., W.A.J.B., F.H., R.C., G.R.T., S.M., R.E., K.S.-L., and C.H. wrote the manuscript; J.A.A.C.H., M.M., G.J.G., F.H., and P.C.G.H. designed the research; H.W.G., J.A.A.C.H., G.J.G., W.A.J.B., R.C., and F.H. performed the research; H.W.G., J.A.A.C.H., and W.A.J.B. analyzed the data.

© 2019 The Authors *Clinical Pharmacology & Therapeutics* © 2019 American Society for Clinical Pharmacology and Therapeutics

- Kelliher, M.A., Seldin, D.C. & Leder, P. Tal-1 induces T cell acute lymphoblastic leukemia accelerated by casein kinase IIalpha. *EMBO J.* **15**, 5160–5166 (1996).
- Ting, A.T., Pimentel-Muñoz, F.X. & Seed, B. RIP mediates tumor necrosis factor receptor 1 activation of NF-kappaB but not Fas/APO-1-initiated apoptosis. *EMBO J.* **15**, 6189–6196 (1996).
- Degterev, A. et al. Identification of RIP1 kinase as a specific cellular target of necrostatins. *Nat. Chem. Biol.* **4**, 313–321 (2008).
- Degterev, A. et al. Chemical inhibitor of nonapoptotic cell death with therapeutic potential for ischemic brain injury. *Nat. Chem. Biol.* **1**, 112–119 (2005).
- Re, D.B. et al. Necroptosis drives motor neuron death in models of both sporadic and familial ALS. *Neuron* **81**, 1001–1008 (2014).
- Najjar, M. et al. Structure guided design of potent and selective ponatinib-based hybrid inhibitors for RIPK1. *Cell Rep.* **10**, 1850–1860 (2015).
- Qiu, X. et al. CD40 ligand induces RIP1-dependent, necroptosis-like cell death in low-grade serous but not serous borderline ovarian tumor cells. *Cell Death Dis.* **6**, e1864 (2015).
- Cognoux, A. et al. Necroptosis in Niemann–Pick disease, type C1: a potential therapeutic target. *Cell Death Dis.* **7**, e2147 (2016).

- Smith, C.C. et al. Necrostatin: a potentially novel cardioprotective agent? *Cardiovasc. Drugs Ther.* **21**, 227–233 (2007).
- Lukens, J.R. et al. RIP1-driven autoinflammation targets IL-1alpha independently of inflammasomes and RIP3. *Nature* **498**, 224–227 (2013).
- Liu, M. et al. Necroptosis, a novel type of programmed cell death, contributes to early neural cells damage after spinal cord injury in adult mice. *J. Spinal Cord Med.* **38**, 745–753 (2015).
- Ofengeim, D. et al. Activation of necroptosis in multiple sclerosis. *Cell Rep.* **10**, 1836–1849 (2015).
- Su, X. et al. Necrostatin-1 ameliorates intracerebral hemorrhage-induced brain injury in mice through inhibiting RIP1/RIP3 pathway. *Neurochem. Res.* **40**, 643–650 (2015).
- Yin, B. et al. Inhibition of receptor-interacting protein 3 upregulation and nuclear translocation involved in necrostatin-1 protection against hippocampal neuronal programmed necrosis induced by ischemia/reperfusion injury. *Brain Res.* **1609**, 63–71 (2015).
- Viringipurampeer, I.A. et al. NLRP3 inflammasome activation drives bystander cone photoreceptor cell death in a P23H rhodopsin model of retinal degeneration. *Hum. Mol. Genet.* **25**, 1501–1516 (2016).
- Caccamo, A. et al. Necroptosis activation in Alzheimer's disease. *Nat. Neurosci.* **20**, 1236 (2017).
- Ofengeim, D. et al. RIPK1 mediates a disease-associated microglial response in Alzheimer's disease. *Proc. Natl. Acad. Sci. USA* **114**, e8788–e8797 (2017).
- Weisel, K. et al. Randomized clinical study of safety, pharmacokinetics, and pharmacodynamics of RIPK1 inhibitor GSK2982772 in healthy volunteers. *Pharmacol. Res. Perspect.* **5**, e00365 (2017).
- David, S. & Hamilton, J.P. Drug-induced liver injury. *US Gastroenterol. Hepatol. Rev.* **6**, 73–80 (2010).
- Danan, G. & Teschke, R. RUCAM in drug and herb induced liver injury: the update. *Int. J. Mol. Sci.* **17**, 14 (2016).
- Maria, V.A. & Victorino, R.M. Development and validation of a clinical scale for the diagnosis of drug-induced hepatitis. *Hepatology* **26**, 664–669 (1997).
- Berger, S.B. et al. Cutting edge: RIP1 kinase activity is dispensable for normal development but is a key regulator of inflammation in SHARPIN-deficient mice. *J. Immunol.* **192**, 5476–5480 (2014).
- Newton, K. et al. RIPK3 deficiency or catalytically inactive RIPK1 provides greater benefit than MLKL deficiency in mouse models of inflammation and tissue injury. *Cell Death Differ.* **23**, 1565–1576 (2016).
- Liu, Y. et al. RIP1 kinase activity-dependent roles in embryonic development of Fadd-deficient mice. *Cell Death Differ.* **24**, 1459–1469 (2017).
- Yoon, E. et al. Acetaminophen-induced hepatotoxicity: a comprehensive update. *J. Clin. Transl. Hepatol.* **4**, 131–142 (2016).
- Björnsson, E.S. Drug-induced liver injury due to antibiotics. *Scand. J. Gastroenterol.* **52**, 617–623 (2017).
- Sulkowski, M.S. Drug-induced liver injury associated with antiretroviral therapy that includes HIV-1 protease inhibitors. *Clin. Infect. Dis.* **38**(Suppl. 2), S90–S97 (2004).
- Björnsson, E., Olsson, R. & Remotti, H. Norfloxacin-induced eosinophilic necrotizing granulomatous hepatitis. *Am. J. Gastroenterol.* **95**, 3662–3664 (2000).
- Jin, Y. et al. Dose-dependent acute liver injury with hypersensitivity features in humans due to a novel microsomal prostaglandin synthase 1 inhibitor. *Br. J. Clin. Pharmacol.* **84**, 179–188 (2018).
- Takemoto, K. et al. Necrostatin-1 protects against reactive oxygen species (ROS)-induced hepatotoxicity in acetaminophen-induced acute liver failure. *FEBS Open Bio.* **4**, 777–787 (2014).
- Filliol, A. et al. RIPK1 protects from TNF-α-mediated liver damage during hepatitis. *Cell Death Dis.* **7**, e2462 (2016).
- Zhang, D.W. et al. RIP3, an energy metabolism regulator that switches TNF-induced cell death from apoptosis to necrosis. *Science* **325**, 332–336 (2009).
- Pasparakis, M. & Vandenabeele, P. Necroptosis and its role in inflammation. *Nature* **517**, 311–320 (2015).